Simulation of Flow and Mixing of Particles in a Rotating and Rocking Cylinder

Carolyn Wightman, Maher Moakher, and Fernando J. Muzzio
Dept. of Chemical and Biochemical Engineering, Rutgers University, Piscataway, NJ 08855

O. Walton
Dept. of Mechanical Engineering, University of Florida, Gainesville, FL 32611

Granular material in a cylindrical vessel undergoing rotational and rocking motions is modeled using a discrete element method. Rotational motion supplemented by rocking is compared to purely rotational motion via linear density profiles, velocity fields, and axial concentration profiles. The rocking motion, which imparts a time-dependent flow perturbation to purely rotational motion, dramatically enhanced mixing in laboratory studies. Simulation results appear to agree well with experimental results and observations.

Introduction

Many technical fields deal with mixing of granular materials, including chemical, agricultural, ceramic, mechanical, civil and soil engineering, the life sciences, physics, and pharmacy. Although researchers in these fields consider a wide range of physical characteristics and flow regimes, they share a common interest: the need to understand and characterize bulk-flow powder behavior. Powder processing has been recently characterized by chemical engineers as having a legacy of neglect (Ennis et al., 1994). Awareness of this neglect has motivated a recent resurgence of both experimental investigations (McCarthy et al., 1996; Hill and Kakalios, 1995; Brone et al., 1997) and theoretical approaches (Johnson et al., 1990; Edwards and Mounfield, 1996). It has become fashionable in a sense to study powders, not only because of their complexity but also because there is a growing need in industry to reliably manufacture high-quality products.

Although practitioners have attempted to handle powder problems using empirical approaches, more detailed studies of the physics of powders are required. Some researchers have suggested that granular materials might be a different state of matter (Jaeger et al., 1996). Interest in the physics of powders has increased dramatically in the past decade, starting with the analysis of sand piles (Baxter et al., 1989, 1993; Bak and Chen, 1991), prompted by analogies with self-organized critical systems (Bak et al., 1988). Fundamental questions concerning how and why granular materials behave alternatively like a liquid when flowing down an inclined chute and like a solid when forming a sloping surface remain to be answered (Glanz, 1995). A growing research community is currently investigating microscopic theories (Jaeger et al., 1996; Jaeger and Nagel, 1992; Evesque and Stefani, 1991; Evesque et al., 1992; Mehta, 1994), as well as unit operations typically found in industry, such as blending, sampling, discharge, fluidization, and granulation. The kinetic theory developed for fast-flowing low-density solids has achieved some success in modeling Couette flows and flows down inclined planes, but industrial systems are often more complex. Civil and soil engineers are mainly interested in strain effects (failure) produced by external forces and the effect of time on the development of strain. The chemical engineering community, on the other hand, has focused primarily on mixing and transport. For example, a mixing question concerning the production of pharmaceutical tablets is whether a multicomponent batch of material is sufficiently mixed to meet imposed tolerances. A common approach to powder blending is to use a tumbling blender, which is essentially a hollow vessel attached to a horizontal rotating shaft. While efforts have been made to design mixing processes that maximize homogeneity and minimize mixing times, mixers are usually designed by trial and error, and mixing flows within them are poorly understood.

It was found in laboratory studies that time-dependent flow perturbations can dramatically enhance mixing in granular systems. Previous experimental studies (Wightman and

Correspondence concerning this article should be addressed to F. J. Muzzio.

Muzzio, 1997; Wightman et al., 1995) showed that application of small-amplitude vertical rocking motion resulted in very significant enhancements in the axial mixing rate in a rotating cylinder. In this article, discrete element simulations are used to gain further insight into the effects of rocking flow perturbations. Granular mixing inside a cylinder that rotates about a horizontal axis and rocks in the vertical direction is adopted as a case study. After a brief review of directly relevant recent literature, the discrete element method (DEM) is briefly described. The main parameters affecting mixing performance and their results are also discussed.

Background

An important fundamental step toward the full control of powder-mixing processes is to understand the dynamic motion of particles within blenders. In recent years there has been considerable work in this direction. A recent survey of computer simulations dealing with granular materials, structures, flows, and vibrations is given by Barker (1994). Many theories have been proposed to model the dynamic behavior of the granular materials. Most of the models that have been developed fall into three categories: continuum approaches, kinetic theory, and discrete models.

Continuum models are based on the general principles of continuum mechanics. Individual particles are ignored, and it is assumed that the granular material consists of continuous matter that obeys conservation of mass, momentum, and energy. The behavior of the material is then described by constitutive equations. These equations often fail to take into account real material parameters such as plasticity, compressibility, and cohesiveness, and experimental data needed to calculate required parameters and to test continuum theories are not available.

Models based on kinetic theory, which exploit similarities between the interacting grains in a granular material and the colliding molecules in a dense gas, work well when the material behaves like a liquid, for example, for noncohesive materials flowing down inclined chutes, but fails when the material shows nonfluid characteristics, such as the formation of a sloped surface.

Discrete models such as the one used in this article consider the granular material as a collection of a large number of discrete solid particles that move independently from one another. The simulation algorithm, which is known as the discrete element method (DEM), was originally developed by Cundall and Strack (1979), and models granular systems as a collection of discrete particles that move as a result of globally applied forces (such as gravity) and interact through surface contacts. In principle, simulated particles can have any shape, such as disks, spheres, or polygons, but complicated shapes increase the complexity of the algorithm for contact detection and add to the computational cost. The major drawback to this approach is the extremely large computer resources required even for relatively small numbers of particles.

The flow of granular material in a rotating cylinder, the case considered in this article, has been modeled by several investigators (Mishra and Rajamani, 1990; Walton and Braun, 1993; Ristow, 1994; Buchholtz et al., 1995; McCarthy et al., 1996). Walton and Braun (1993) examined rotation rates from quasi-static to centrifugal. Using both round and square particles, they performed computations that predicted the angle of repose as a function of interparticle friction and rotation speed. Mishra and Rajamani (1990) simulated media motion in a ball mill in two dimensions and compared results with experiments. One comparison showed that the position of two arbitrary balls can be accurately tracked and matched to the simulated trajectories. Buchholtz et al. (1995) performed 2-D simulations with square particles in a circular mixer, and Baumann et al. (1995) used segregating assemblies. McCarthy et al. (1996) examined traverse (cross-sectional) mixing in a slowly rotating, quasi-2-D cylinder using mixtures of small cubic particles as well as large spherical particles. Algorithms to handle more complicated particle geometries have also been developed. Ghaboussi and Barbosa (1990) presented a 3-D model where individual grains are represented as rigid hexagonal solids that can rotate and undergo different types of contact. More recently, Hogue and Newland (1994) modeled contact detection for 2-D irregular-shape particles. So far, DEM has been applied to realistic engineering problems in just a few cases. Researchers have typically limited their work to at most a few thousand particles of simple shape in geometries. All of the studies mentioned earlier were either strictly 2-D (planar particles in a planar flow domain) or quasi-2-D (shallow cylinders with periodic boundary conditions in the axial direction). To the best of our knowledge, this article describes the first simulation of a nontrivial 3-D velocity field (combination of axial rotation and vertical rocking) in a fully 3-D geometry (a long cylinder with rotating axial boundary conditions).

Discrete-Element-Method Simulations

The computer models and algorithms used here were originally developed at the Lawrence Livermore National Laboratory (Walton, 1993b). In all the simulations reported in this article, particle trajectories are obtained by solving Newton's equation of motion, $m(dv/dt) = \Sigma F$. Particles are allowed to overlap at contact points where it is assumed that particle deformation is negligible compared to the particles' displacements as rigid bodies. Each particle in the simulated system may interact with its neighbors or with the boundary only at contact points through normal and tangential forces. The normal forces between pairs of particles in contact are calculated using either Hertz's impact theory (Walton, 1993) or the partially latching spring model of Walton and Braun (1986). Inelasticity of collisions is incorporated into simulations by including a coefficient of restitution e, defined as the negative of the ratio of the recoil to incident speeds in the normal direction. Contact forces are calculated using a bilinear spring model for the normal-direction force and a nonlinear, hysteretic model for the tangential force. Stiffness coefficients are chosen to be large enough to ensure that overlap remains small compared to particle size. Tangential contact forces are calculated using the incremental slipping model of Walton and Braun (1986). After contact occurs, tangential forces build up nonlinearly, causing displacements in the tangent plane of contact. The initial tangential stiffness is taken to be a fraction of the normal stiffness. A Coulomb-type friction law is assumed to apply; if the calculated magnitude of the shear

15475905, 1998, 6, Downloaded from https://aiche.onlinelibrary.wiley.com/doi/10.1002/aic.690440605 by Universitá© De Nantes, Wiley Online Library on [13/10/2026]. See the Terms and Conditions (https://onlinelibrary.wiley.com/terms-and-conditions) on Wiley Online Library for rules of use; OA articles are governed by the applicable Creative Commons License

force at contact points exceeds the product of the normal force and the coefficient of friction, sliding occurs. The resultant force on each particle is given by the sum of all the contact forces and the gravitational force, and the resultant torque is calculated from the tangential contact forces.

Newton's second law is expressed as a first-order differential system of equations for positions and velocities:

$$\frac{dr(x,y,z)}{dt} = v(x,y,z)$$

$$\frac{dv(x,y,z)}{dt} = g(x,y,z) + \frac{F(x,y,z)}{m}. \qquad (1)$$

Assuming the contact forces, $F(x,y,z)$, to be constant during a time step, the system is integrated forward in time using a central difference scheme. Particle positions are calculated at each time step, and velocities are calculated at half time steps, forward in time using a "leap frog" method (Allen and Tildesley, 1987). Euler's equations of motion are also integrated using a similar algorithm. Only the angular velocities are integrated, since the angular displacements need not be integrated for spherical particles. Due to the explicit nature of the integration scheme, to achieve reasonable accuracy and preserve numerical stability, the time step is a small fraction of the critical time step (Walton and Braun, 1986) and is on the order of 10^{-5} s.

In order to minimize the amount of time spent detecting contacts, a Verlet's list of neighbors is constructed (Allen and Tildesley, 1987). Particles located within a "cutoff" distance from a given particle are considered to be elements of that particle's neighbor list. This concept is illustrated in Figure 1, where particles 3, 4 and 5 are elements of particle 1's neighbor list. Contacts with a given particle are sought only among the elements of its neighbor list. This list is constructed at the beginning of the simulation and updated whenever a particle moves a distance greater than half the cutoff distance from the last update (approximately every ~1,000 time steps). Although DEM is more physically realistic than continuum approaches, it currently requires extensive computer resources to simulate physically meaningful numbers of particles. Simulations of just 10,000 particles, with properties as described in Table 1, take ~48 h of CPU time for 1 s real time on a Sun SPARC 20.6 workstation.

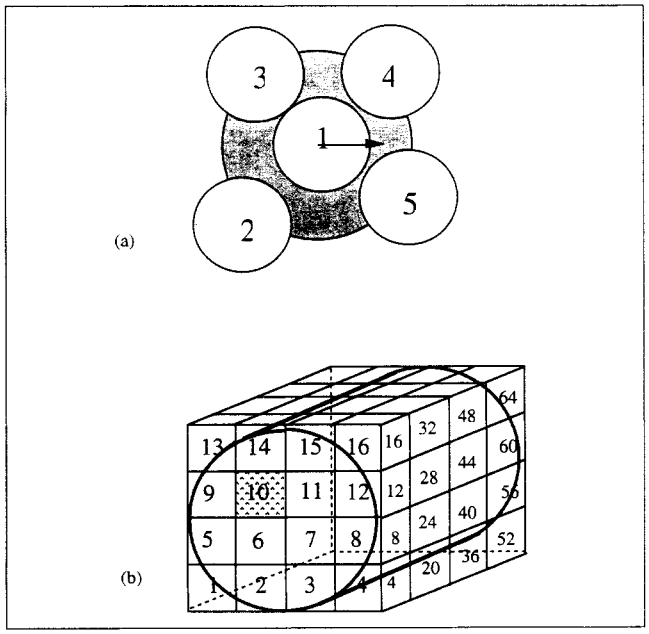

Figure 1. Cutoff sphere for particle 1, with particles 3, 4, and 5 in its neighbor list.

Table 1. Summary of the Simulation Runs Discussed in This Article

No. of Particles	Pure Rotat. Motion	Rocking Freq. ($\beta = -10°$ Rock.)	Fill Fraction J
10,000	$\Omega = 0$	$\Omega = 1, 2$	0.28
	$\Omega = 0$	$\Omega = 1$, 1.8 and 2	0.36
	$\Omega = 0$	$\Omega = 1$, 1.8 and 2	0.40
	$\Omega = 0$	$\Omega = 1, 2$	0.50
25,000	$\Omega = 0$	$\Omega = 1, 2$	0.50

The mixing vessel considered here is a 3-D rotating horizontal drum partially filled with inelastic, frictional spherical particles. Solid rotating boundaries at both ends of the cylinder are used here to increase relevance and realism. While the presence of end walls both adds complications to the simulation of particle motion (due to particle-boundary interactions) and emphasizes the finite size of the simulations, the presence of end walls approximates experimental conditions more closely than periodic boundaries.

Rocking motion is incorporated into the simulation by rotating the gravity vector with a sinusoidal time-dependent function (Figure 2a). This technique is only valid if the inertial effect of the vertical motion at the ends of the rocking cylinder can be neglected. In the simulations in this article, the maximum vertical acceleration of the end of the rocking cylinder was less than 1.25×10^{-3} g. A rocking cycle is defined as the downward pivot of the vessel and its return to the horizontal position. The rocking motion is characterized by the parameter Ω, defined as the number of rocking cycles per revolution. Figure 2b depicts the magnitude of the rocking angle and the corresponding gravity force along the axis in the x-direction. Herein we investigate the effects of varying the rocking frequency Ω on both radial and axial mixing.

Conditions/parameters

Computer simulations reported here consider a horizontal drum mixer with a diameter of 126 mm (106 mm diameter is used in one simulation). The vessel is loaded with 10,000 to 25,000 spherical particles with a uniform diameter of 3.78 mm, giving 25 to 50 particle diameters in the axial direction. The speed of rotation is kept constant at $\omega = 1.57$ rad/s (15 rpm) in all simulations. This speed corresponds to about 13% of the critical speed of 119 rpm. Table 1 shows a list of cases considered in this article.

The data structure for each particle includes its shape, size, density, moment of inertia about its center of mass, coefficient of restitution, particle–particle friction coefficient, particle–wall friction coefficient, position, velocity, and orientation. These conditions determine the outcome of the

15475905, 1998, 6, Downloaded from https://aiche.onlinelibrary.wiley.com/doi/10.1002/aic.690440605 by Universitè De Nantes, Wiley Online Library on [13/10/2026]. See the Terms and Conditions (https://onlinelibrary.wiley.com/terms-and-conditions) on Wiley Online Library for rules of use; OA articles are governed by the applicable Creative Commons License

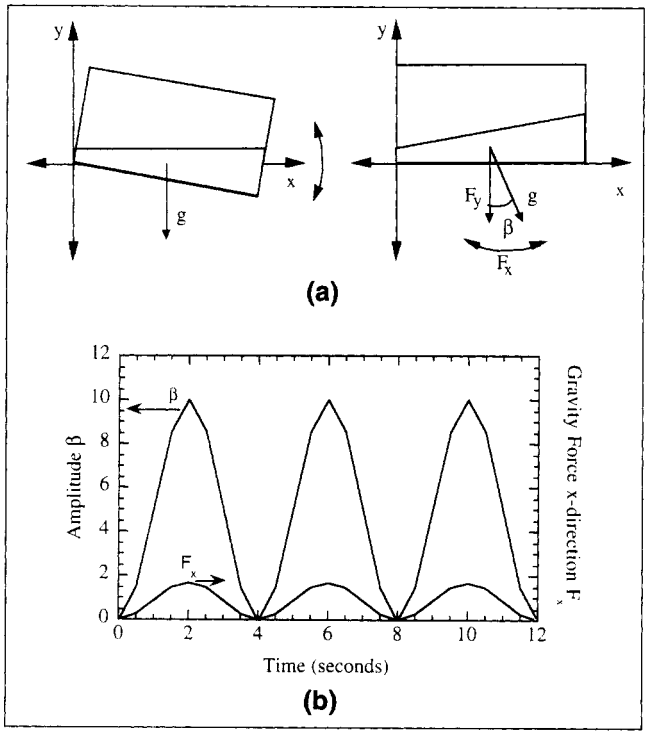

Figure 2. (a) Experimental rocking motion (left) with the drum tilted by an angle β and returned to the horizontal position in one rocking cycle, and the computational rocking motion (right) with rocking modeled by rotating the gravity vector; (b) magnitude of rocking angle β and the corresponding gravity force along the axis in the x-direction for $\Omega = 1$.

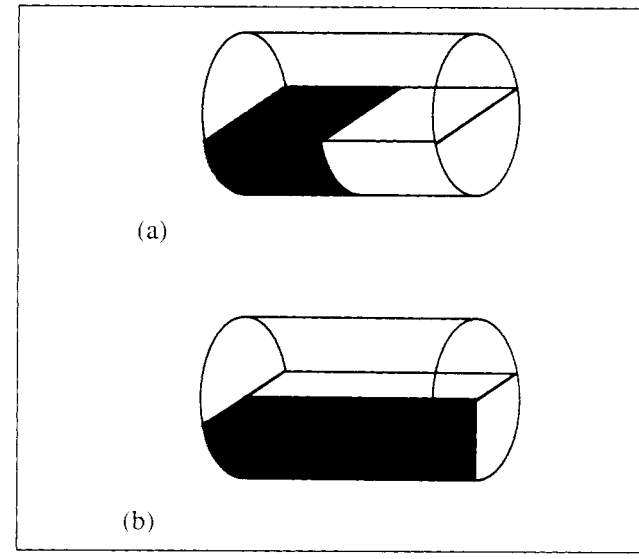

Figure 3. Tagging conditions for two loading strategies: (a) front-to-back and (b) side-by-side.

simulation. Parameters required in the normal and tangential force models are the coefficient of restitution, normal stiffness, interparticle friction, particle–wall friction, and tangential stiffness. Table 2 summarizes the parameters assigned at the start of the simulation. The particles are assigned a restitution coefficient equal to 0.85 that is similar to that of glass beads (Walton and Braun, 1993), an interparticle friction coefficient, $\mu_p = 0.4$, and a particle–wall friction coefficient, $\mu_w = 1.0$, that are based on Walton and Braun's data relating the angle of repose to the friction coefficient and rotational speed (Walton and Braun, 1986, 1993; Walton, 1993). In one simulation case, the particle–wall friction coefficient is reduced to 0.4.

Table 2. Parameter Values Used in the Simulations

Parameter	Symbol	Assigned Value
Particle diameter	dp	3.78 mm
Drum diameter	D	106; 126 mm
Particle density	ρ_p	2.5 g/cm^3
Coeff. of restitution	e	0.85
Normal-force coeff.	K_1	2,000
Tangential/normal stiffness	K_0/K_1	0.7
Particle–particle friction coeff.	μ_p	0.4
Particle–wall friction coeff.	μ_w	0.4; 1.0
Rocking frequency	Ω	0, 1, or 2
Rotation rate	ω	1.57 rad/s

Velocity profiles, mixture patterns, and mixing performance are examined for 50:50 mixtures of components that differ only by color. First, the particles are randomly loaded into the bottom half of the horizontal drum, and assigned an average initial velocity that facilitates gravitational settling. Particles are tagged by color based on their location. At $t = 0$ s, the cylindrical boundary begins rotating. Two tagging strategies are used to mimic different experimental initial conditions: front-to-back (Figure 3a) and side-by-side (Figure 3b). Since the particles move slightly during the settling process, tagging is performed at $t = 0.5$ s for front-to-back loading. The main features of the flow (solid body rotation in the lower portion of the bed, cascading motion on the upper surface) develop within 0.5 s.

Due to computational limitations, simulations are restricted to a much smaller number of particles than in previously communicated laboratory experiments (Wightman and Muzzio, 1997; Wightman et al., 1996). Hence, to allow closer comparison, additional experiments were carried out using modified conditions. Commercially available 4-mm red and blue spherical glass beads (Jaygo, New Jersey) were loaded into a 106×140-mm drum vessel in a side-by-side configuration. The mixtures were solidified with gelatin, subsequently sliced, and compared with a simulation using 10,000 spherical particles for the parameters shown in Table 2.

Results and Discussion

Velocity profiles for pure rotation

Given that the time step is on the order of 10^{-5} s, and that position and velocity updates are performed for every time step, the instantaneous snapshot of the velocity field, computed as the time derivative of position, shows a great deal of variability. To obtain a more meaningful depiction of the flow, a spatially and temporally averaged velocity field is computed, obtaining a much smoother result. First, the domain is divided into zones slightly smaller than the particles themselves. The velocity of particles visiting each zone is recorded

15475905, 1998, 6, Downloaded from https://aiche.onlinelibrary.wiley.com/doi/10.1002/aic.690440605 by Universitã© De Nantes, Wiley Online Library on [13/10/2026]. See the Terms and Conditions (https://onlinelibrary.wiley.com/terms-and-conditions) on Wiley Online Library for rules of use; OA articles are governed by the applicable Creative Commons License

and averaged over many time steps. The averaged velocity field of the cascade layer, viewed along the axis of the cylinder for purely rotational motion ($\Omega = 0$), is shown in Figure 4a. Most of the particles move in parallel paths from the top to the bottom of the cascade. This pattern is well known from experimental work (Hogg et al., 1966; Lacey, 1945). Axial movement occurs as a result of instantaneous impact collisions. Cross-sectional averaged velocity profiles for pure rotation ($\Omega = 0$) are shown in Figures 4b–4f for varying fractions of fill volume $J = 0.28$, 0.36, 0.40, 0.50, and 0.66, respectively. All runs involve 10,000 particles. To keep the number of particles constant, the length of the vessel varies to corresponding values of 142, 119, 102, 80, and 62 mm. For low fillings ($J = 0.28$), the profiles depict a thin layer of particles traveling with the rising drum wall. Particles immediately above this layer also move in the direction of the rotating drum, but rotation is disordered and intermingling occurs between layers. The moving layers reach the surface and slump downwards over the particles moving upward. The bed exhibits movement between layers along with recirculation patterns. Observations in the laboratory with 4-mm glass beads at the same rotation rate (15 rpm) confirm both the presence of the layer adjacent to the wall and the slumping motion on top of the cascade.

A more regular cascade and an off-center recirculation pattern are observed in Figure 4c for a fill fraction of $J = 0.36$.

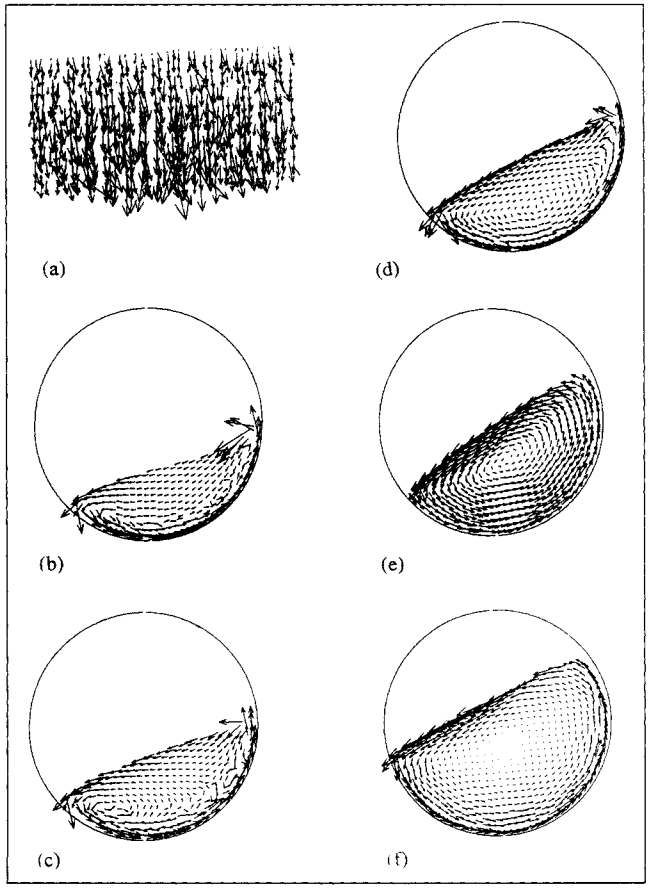

Figure 4. Average velocity field for pure rotation.

The figure shows (a) the cascade region for $J = 0.5$ and also cross sections of the mixer for fill fractions of (b) $J = 0.28$, (c) 0.36, (d) 0.40, (e) 0.50, and (f) 0.60.

The thin layer of particles rotating with the wall is also apparent, and likely due to $\mu_w > \mu_p$. Above this layer and in the upper half of the bed, the particles appear to intermingle between layers. For $J \geq 0.40$, a transition occurs, and the velocity field shows orderly solid-body rotation through most of the bed, as well as a smooth, continuously flowing cascade at the free surface. A stagnation point develops at the center of the lower boundary of the cascade region, surrounded from below by particles moving in solid-body rotation and from above by a layer of particles streaming at the cascade region; however, for filling levels $J < 0.50$, the cascade layer intersects the solid-body rotation trajectories, and no stagnant region exists in the vessel. In Figure 4d the cascade layer appears to be ~ 4 particles thick. Each vector in Figure 4 represents a particle, and the measure of the layer thickness can be accomplished by connecting vectors (streamlines) in the quiver diagrams. Laboratory observations with 4-mm particles at 15 rpm again confirm these observations: the cascade layer is two to four particles thick, and the inner layers exhibit solid-body rotation. These prominent features of the bulk flow observed in the laboratory agree well with the time-average velocity profiles.

Unlike observations at lower fillings, at $J = 0.50$ both the average and the instantaneous velocity profiles reveal a smooth bulk flow (Figure 4e). The rotating bed moves with solid-body rotation, and both a well-developed cascade and nearly stagnant central core zone develop. There is minimal mixing between layers as they move in solid-body rotation with the wall. Because the bulk-flow pattern is smooth and well-organized, these observations are easily confirmed in laboratory experiments. Using an image-processing device to examine a 2-D rotating cylinder filled with 3-mm steel balls, Rajchenbach et al. (1993) measured velocity fields that appear very similar to those shown in Figure 4e.

For filling levels $J > 0.50$, another transition occurs. Figure 4f shows the velocity field obtained for $J = 0.66$. Although the velocity profile depicts the same number of layers undergoing solid-body rotation as in the previous case, a stagnant core region is observed at filling levels $J > 0.50$. For such cases, the cascading region ends above the stagnation point. Particles close to the stagnation point travel along closed solid-body rotating trajectories in a circular pattern consistent with observations made by other investigators (Hogg and Fuerstenau, 1972), and do not experience convective mixing with the surrounding granular material. Only dispersive mixing mechanisms are available to such particles, and under such conditions cross-sectional mixing is much slower. As the filling level increases further, the stagnant core grows in size and the cascade layer decreases in depth; both conditions effectively reduce mixing. In laboratory experiments, the cascade has a thickness of one particle diameter at the top of the cascade, grows to approximately three particle diameters in the middle of the cascade, and reduces back to one particle diameter at the bottom. A similar pattern is observed by the simulations in Figure 4f. In summary, a comparison of visual experiments and simulations indicate that the simulations closely predict bulk flow behavior for a number of fill volumes. Imaging photographs of laboratory experiments also agree with these descriptions (Rajchenbach et al., 1993).

Figure 5a shows the cross section of the drum with the particle motion along a vessel diameter perpendicular to the

15475905, 1998, 6, Downloaded from https://aiche.onlinelibrary.wiley.com/doi/10.1002/aic.690440605 by Universitá© De Nantes, Wiley Online Library on [13/10/2026]. See the Terms and Conditions (https://onlinelibrary.wiley.com/terms-and-conditions) on Wiley Online Library for rules of use; OA articles are governed by the applicable Creative Commons License

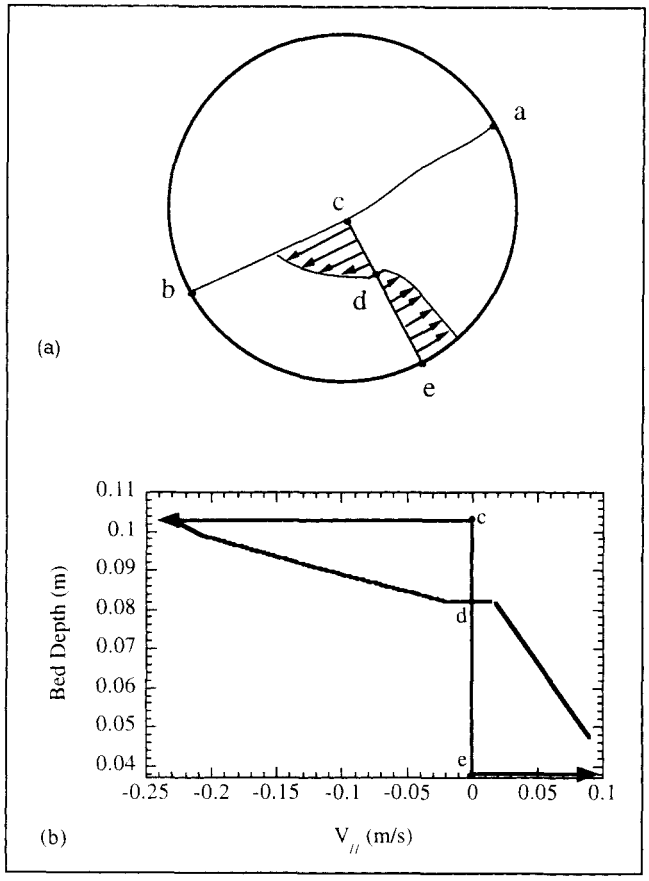

Figure 5. (a) View; (b) measured values of the particle motion parallel to the free surface along a diameter perpendicular to the free surface for $J = 0.5$ at 15 rpm.

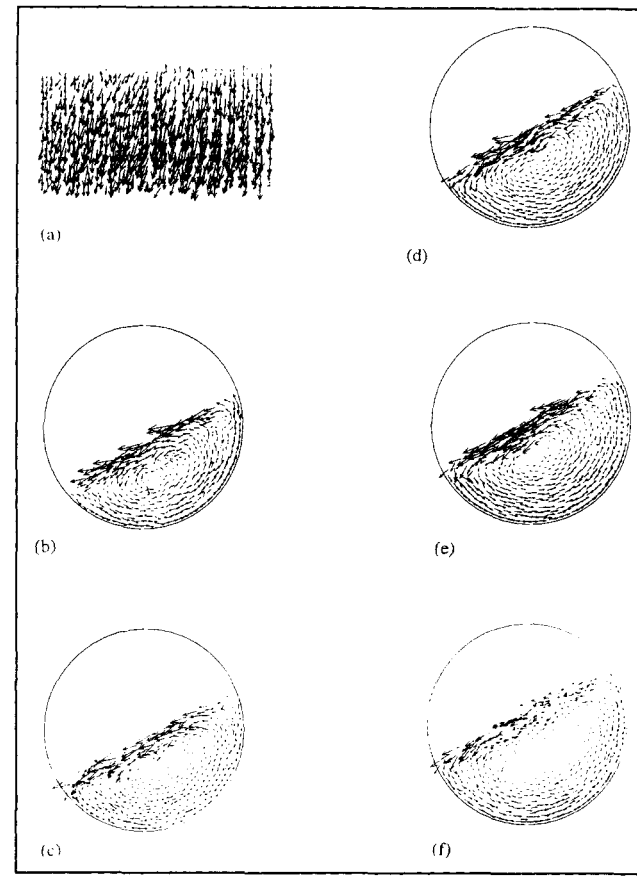

Figure 6. (a) Average velocity in the cascade layer at $\tau = 0.99$ for $\Omega = 2$, $J = 0.5$; (b–f) cross-sectional slices along the axis at (b) 17 mm, (c) 67 mm, (d) 100 mm, (e) 133 mm, and (f) 191 mm.

The rocking motion creates an axial flow in the cascade layer where particles move at an angle across the cascade.

free surface (line *ce*). The actual velocity profile along this line is shown in Figure 5b. At point *d*, there is a discontinuity in the flow where particles above and below point *d* move in different directions. Similar profiles were found by magnetic resonance imaging (MRI) (Nakagawa et al., 1993) and by an imaging device at the end wall (Rajchenbach et al., 1993). Our simulations and these experiments agree in the following aspects: (1) the layer thickness is maximum near the midpoint (point *c*) of the cascade layer, (2) the velocity increases with distance from the boundary between the bed and the cascade layer (point *d*) to the free surface, and (3) the velocity varies across the layer from the top surface angle to the bottom (line *ab*), exhibiting a maximum near the midpoint (point *c*).

Average velocity profiles for rotation with rocking

For the rocking case, $\Omega = 2$, the velocity is again averaged spatially and temporally at corresponding times for every rocking period. Figures 6a–6f show the velocity in the cascade layer (Figure 6a) and at five cross-sectional slices of the mixture (Figures 6b–6f) for $\Omega = 2$ at time $t = 0.99\tau$, where τ is the time for one rocking period. As shown in Figure 6a, the rocking motion creates a net axial flow in the cascade layer where particles move at an angle across the cascade, compared to a nearly straight line flow for $\Omega = 0$. The volume of material at the end of the vessel close to the pivot point decreases during rocking motion (Figure 6b), but the entire bed of particles retains solid-body rotation at this fill level ($J = 0.5$). At the opposite end, particles flow toward and collide with the end wall, creating a temporarily larger stagnant zone

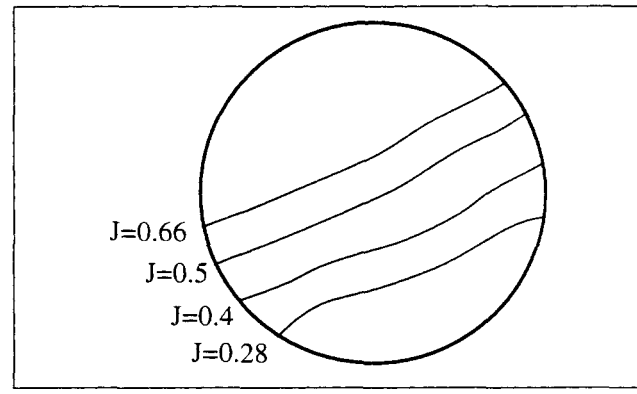

Figure 7. The shape of the free surface for varying fill volumes.

15475905, 1998, 6, Downloaded from https://aiche.onlinelibrary.wiley.com/doi/10.1002/aic.690440605 by Universitá© De Nantes, Wiley Online Library on [13/10/2026]. See the Terms and Conditions (https://onlinelibrary.wiley.com/terms-and-conditions) on Wiley Online Library for rules of use; OA articles are governed by the applicable Creative Commons License

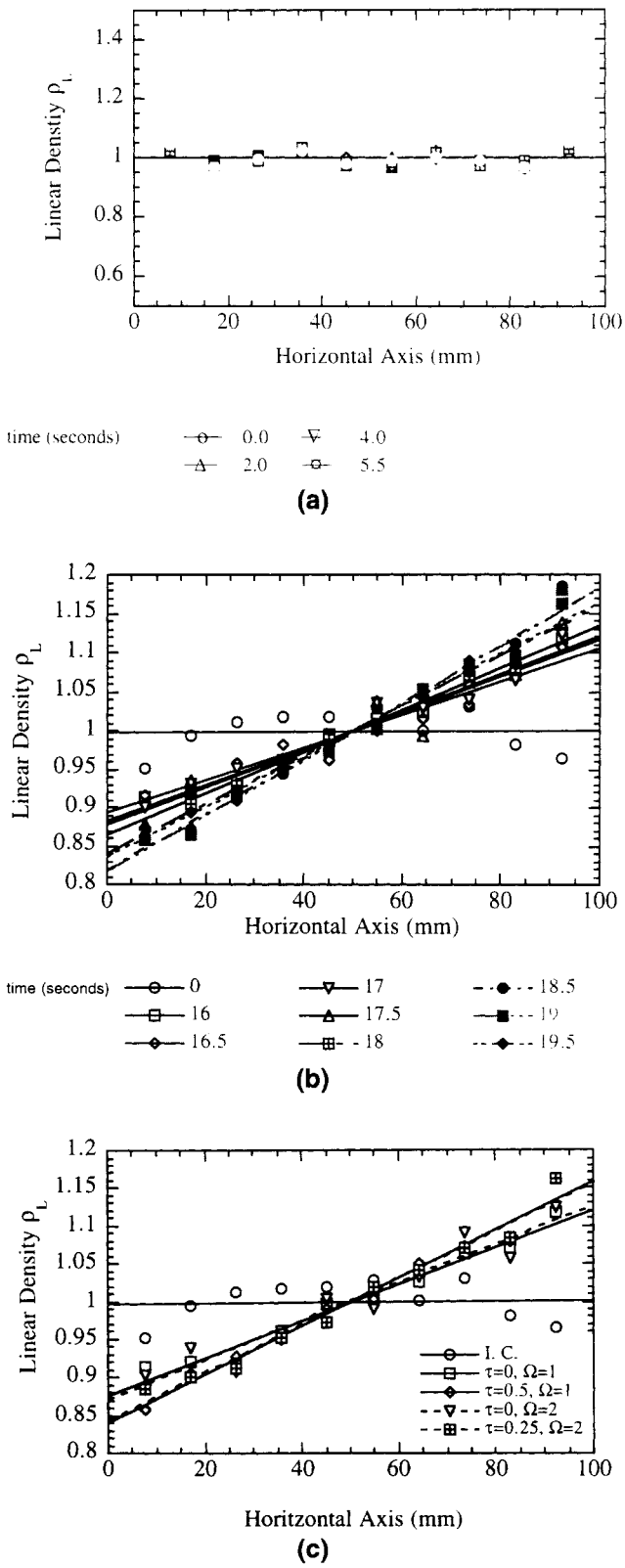

Figure 8. (a) ρ_L vs. position for $\Omega = 0$ from $t = 0$ to 5.5 s; (b) ρ_L for $\Omega = 1$ ($\beta = -10°$, unidirectional rocking).

The open circles are the initial condition. The lines are fitted to ρ_L for one entire rocking cycle. During rocking, ρ_L decreases at one end of the drum and increases at the other end, but it does not revert to a flat uniform profile when the drum returns to the horizontal position.

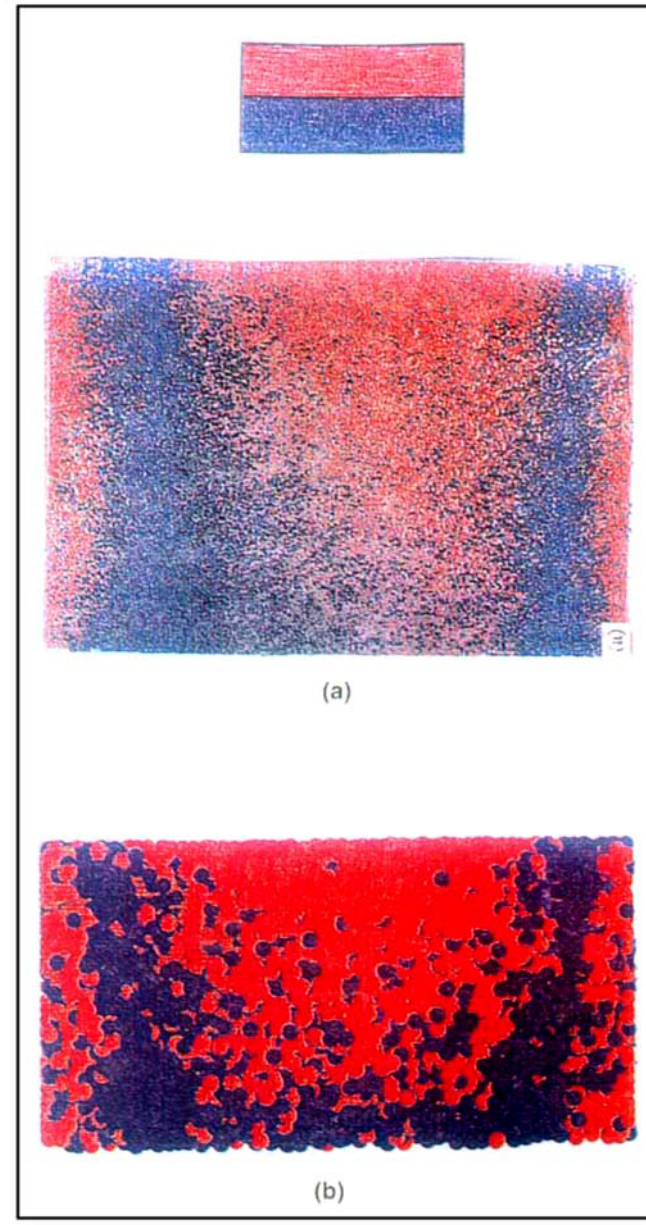

Figure 9. Cascade layers at $N = 3$ revolutions for the side-by-side loading condition for (a) a laboratory experiment and (b) a simulation.

The bands indicate that material near the wall does not necessarily rotate at the same rate as material in the bulk.

(Figure 6f). Compared to pure rotation, the flow is disrupted because the layers form the core shift positions. This bulk-flow effect has a significant impact on axial mixing, as shown later in a comparison of axial concentration profiles in the subsection on mixing dynamics.

Shape of the free surface

Our computations show that the shape of the free surface in the direction of the cascade changes with fill level in a manner similar to experimental observations reported in the literature (Rose and Sullivan, 1958). Figure 7 shows the resultant free-surface shape for varying fill fractions found for

15475905, 1998, 6, Downloaded from https://aiche.onlinelibrary.wiley.com/doi/10.1002/aic.690440605 by Universid© De Nantes, Wiley Online Library on [13/10/2026]. See the Terms and Conditions (https://onlinelibrary.wiley.com/terms-and-conditions) on Wiley Online Library for rules of use; OA articles are governed by the applicable Creative Commons License

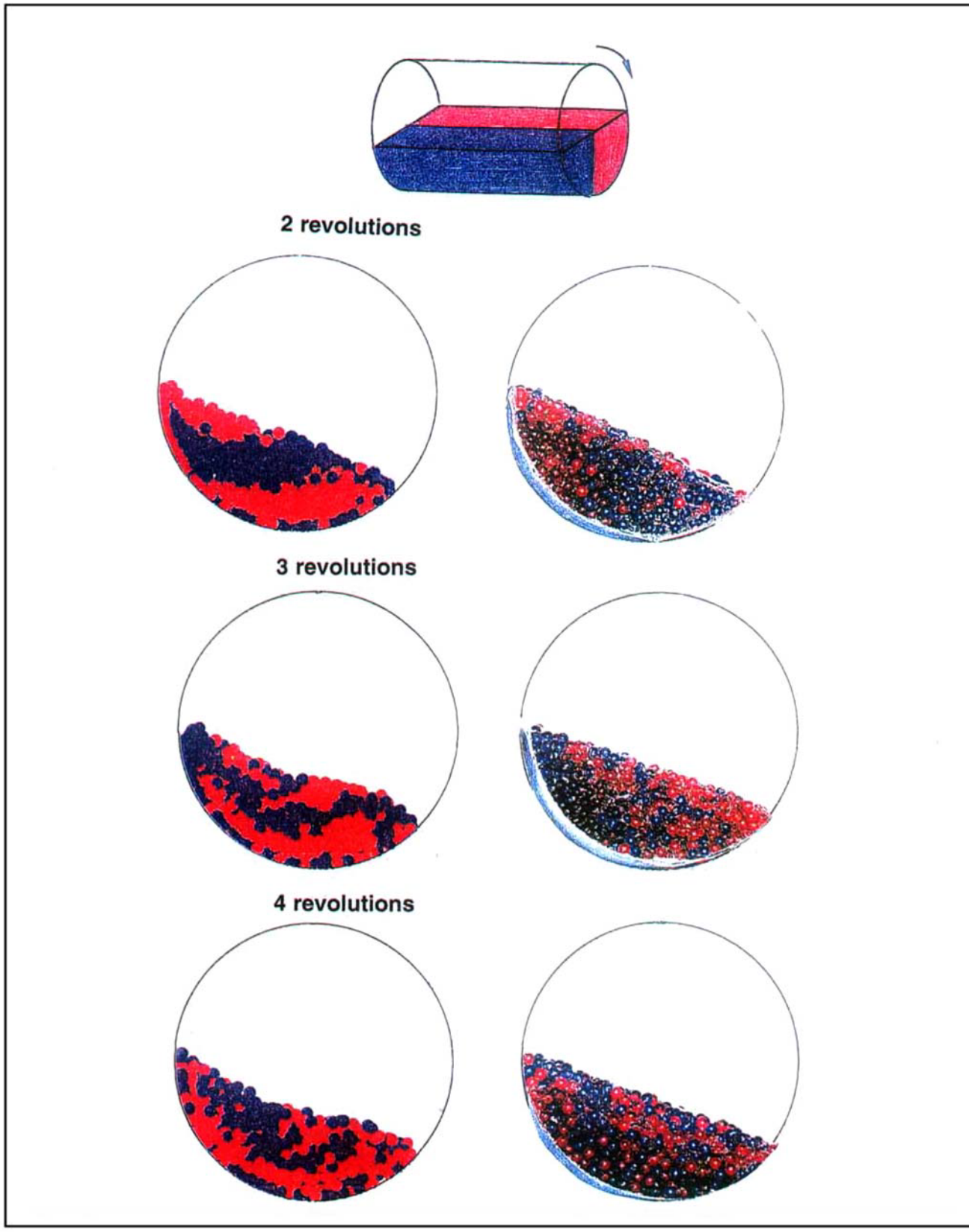

Figure 10. Time evolution of simulations (left) vs. experiments (right) using the same-size particles and vessel diameter.

The particles were loaded side-by-side. At $N = 2$, 3, and 4 revolutions, the cross section in the middle of the mixtures reveals qualitative agreement.

15475905, 1998, 6, Downloaded from https://aiche.onlinelibrary.wiley.com/doi/10.1002/aic.690440605 by Universitè De Nantes, Wiley Online Library on [13/10/2026]. See the Terms and Conditions (https://onlinelibrary.wiley.com/terms-and-conditions) on Wiley Online Library for rules of use; OA articles are governed by the applicable Creative Commons License

15 rpm. For low fillings, such as $J = 0.28$, slumping occurs where particles at the highest point of the surface collectively slump downwards over the bed of particles moving upwards. The shape and slope of the free surface for $J = 0.28$ do not necessarily remain the same over time; however, the sketch shown here is typical of the shape found in the simulations. At higher fill fractions, the free surface is consistently flat during rotation.

The axial variation of the free surface is characterized in terms of the parameter ρ_L, which is defined here as the number of particles per unit of axial length of the vessel, normalized by its average value. Figure 8a shows ρ_L vs. position for $\Omega = 0$ from $t = 0$–5 s (to the best of our knowledge, no experimental results are available to compare with these computational results). For pure rotation, ρ_L is constant; $\rho_L \approx 1$ along the horizontal axis for all times. However, during rocking ρ_L decreases at one end of the drum and increases at the other end. Figure 8b shows ρ_L for $\Omega = 1$ ($\beta = -10°$, i.e., unidirectional rocking) over an entire rocking cycle. The bed does not return to the uniform initial loading condition when the drum returns to the horizontal position. The periodicity of ρ_L closely matches the periodicity of rocking; however, inertial forces cause the minimum and maximum value of ρ_L to occur at $\tau > 0.5$. For example, during the rocking cycle between 16 and 20 s, ρ_L shows a minimum and maximum at 18 to 19 s. For $\Omega = 2$ as shown Figure 8c, ρ_L fluctuates similarly as for $\Omega = 1$.

Mixing patterns for pure rotation

Mixing patterns for pure rotation are shown in Figure 9 for $N = 3$ revolutions, side-by-side initial loading (Figure 3b). The pattern of mixing in the cascade layer is also viewed along the axis of the drum for a laboratory experiment and a simulation (Figures 9a and 9b, respectively). The experiment involves 4,000 μm red and blue particles. The simulation drum considers 25,000 particles ($J = 0.5$), and the mixer length is equivalent to 53 particle diameters. End-wall effects are apparent in the curvature of the initially straight boundary between the red and blue particles. Material at the walls rotates at a different rate than material in the bulk. Particles at the curved surface experience partial slip, while particles at the end wall stick to the wall. The comparison of the patterns shows good qualitative agreement (note that the experiment and simulation involve different-size particles). Cross-sectional slices of the mixtures close to the walls show somewhat different mixing patterns than slices in the center (Wightman et al., 1995), demonstrating that end-wall effects can be significant in both simulations and experiments.

Mixing dynamics

In this section, we use both computational and experimental results to examine the evolution of the mixing process. First, for illustration purposes, simulated and experimental cross-sectional mixing patterns obtained under pure rotational motion (no rocking) using the same-size particles and vessel diameter are shown in Figure 10. The particles are loaded side by side (Figure 3b) with red particles on the right side and blue particles on the left of the initial interface. The drum is rotated clockwise. Figures 10b–10c show both simulated and experimental slices for $N = 2$, 3, and 4 revolutions.

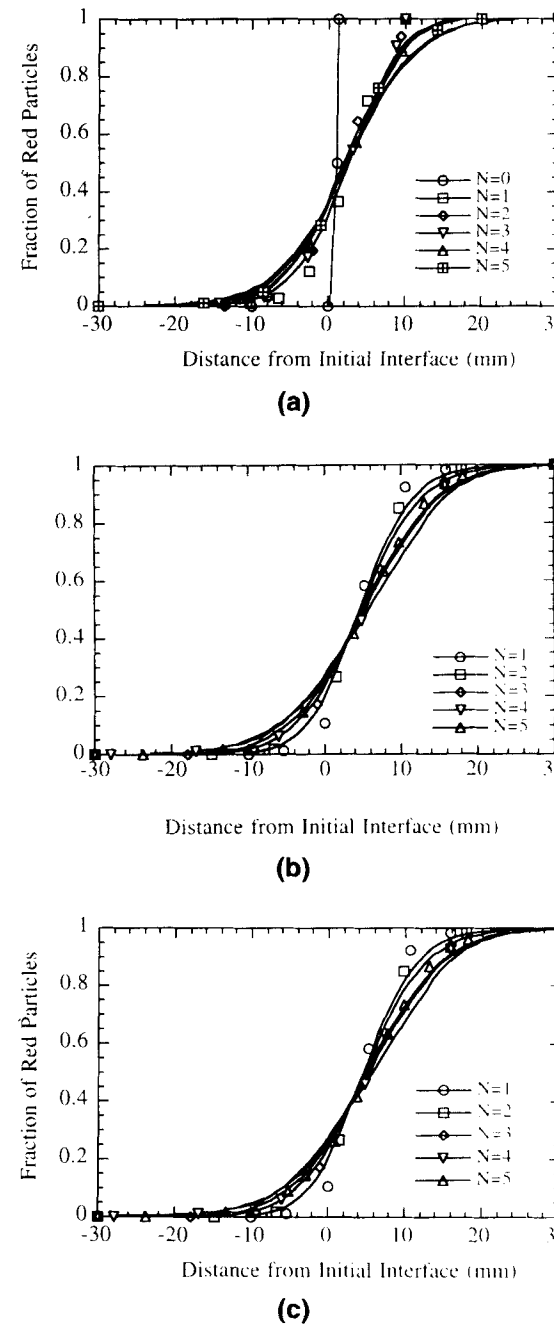

Figure 11. Axial profile of the fraction of red particles vs. initial interface for (a) $\Omega = 0$, (b) $\Omega = 1$, and (c) $\Omega = 2$.

The axial profile confirms laboratory experiments that indicate a trend of enhanced mixing with a time-dependent rocking perturbation. For $\Omega = 0$, very little axial mixing takes place with increasing N. For both $\Omega = 1$ and $\Omega = 2$, the extent of axial mixing increases as N increases.

While experimental and simulated patterns are not identical, the mixtures exhibit good qualitative agreement, indicating that the simulations capture the macroscopic bulk flow of laboratory experiments (the number of particles in each cross section is insufficient to perform a meaningful statistical comparison).

15475905, 1998, 6, Downloaded from https://aiche.onlinelibrary.wiley.com/doi/10.1002/aic.690440605 by Universita' De Nantes, Wiley Online Library on [13/10/2026]. See the Terms and Conditions (https://onlinelibrary.wiley.com/terms-and-conditions) on Wiley Online Library for rules of use; OA articles are governed by the applicable Creative Commons License

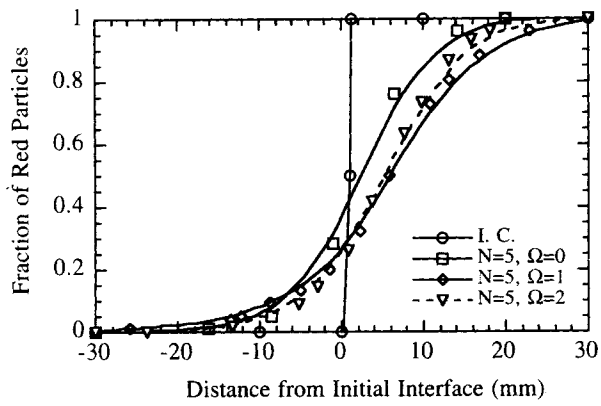

Figure 12. Axial profile of the fraction of red particles vs. initial interface at $N=5$, $\Omega=0$, 1, and 2.

The axial movement of particles starting from a front-to-back condition (Figure 3a) was determined for $\Omega = 0$, 1, and 2 at $N = 0$ to 5 revolutions. Figure 11 illustrates the axial profile where the fraction of red particles is plotted vs. the distance from the initial interface. In agreement with previous experimental work (Wightman and Muzzio, 1997), very little change is observed in the axial profile for $\Omega = 0$. Different behavior is displayed in Figures 11b–11c for $\Omega = 1$ and $\Omega = 2$. In both cases, the axial homogeneity increases with increasing N. In Figure 12 we compare the overall extent of mixing at $N = 5$ revolutions for $\Omega = 0$, 1, and 2. Similar to experiments with 60-μm and 600-μm particles (Wightman et al., 1995; Wightman and Muzzio, 1997), axial mixing is again enhanced by rocking. Experiments for $\Omega = 2$ with 60-μm and $\Omega = 1.8$ with 600-μm particles resulted in significantly faster mixing than for $\Omega = 1$ with both types of particles.

Figure 12 shows experimentally measured axial profiles obtained for $N = 20$ revolutions, $\Omega = 0$, 0.6, 1, 1.8, and 2, using 200-μm particles and a speed of 5 rpm. The figure clearly demonstrates that rocking motion enhances axial mixing; all profiles obtained using rocking motion demonstrate a larger extent of axial homogenization than the profile corresponding to $\Omega = 0$. In Figure 13, $\Omega = 2$ leads to the fastest mixing, followed by $\Omega = 1.8$, 1.0, 0.6, and 0.0 (in that order). The simulation also shows that mixing is enhanced by rocking motion; for both $\Omega = 1$ and $\Omega = 2$ the profiles depart more extensively from the initial steplike condition than for $\Omega = 0$. While in the simulations $\Omega = 1$ gives slightly better mixing than $\Omega = 2$, this difference with experiments can be due to the fact that the simulations correspond to widely different particle sizes (4,000 μm vs. 200 μm) and different rotating speeds (15 rpm vs. 5 rpm). On the other hand, the observed differences may be due to the small number of particles used in the simulations, and it is possible that they would not persist over long times.

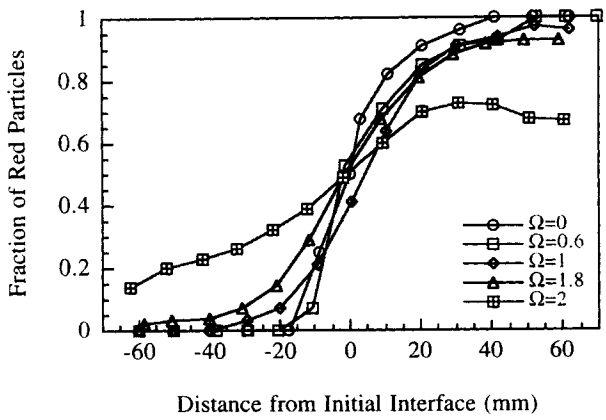

Figure 13. Experimental axial profile of the fraction of red particles vs. initial interface at $N=20$, $\Omega=0$, 0.6, 1, 1.8, and 2 at 5 rpm using 200-μm particles.

For a binary system loaded side by side with different colors, the extent of mixing can be measured in a cross section of the mixer by the number and width of striations, where a striation is defined as a layer of a single color. For short mixing times, the colors are largely segregated from one another and intermingling is limited to a few thin striations located at the boundary between the two colors. Figures 14a and 14b illustrate the cross section of the drum at $x = 0.03$ m for $\Omega = 0$ and $\Omega = 1$ at $N = 2$. Although the number of striations is the same for $\Omega = 0$ and $\Omega = 1$, the striations are stretched thinner for $\Omega = 1$ compared with $\Omega = 0$. For smaller particles, we would expect an intermeshing pattern of increasingly thinner

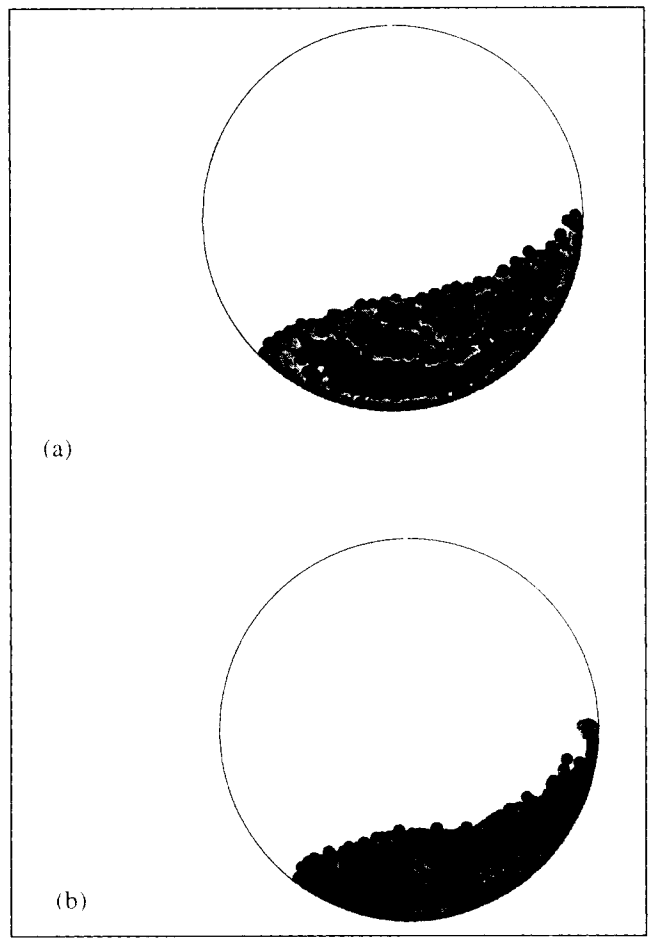

Figure 14. For side-by-side initial loading, the cross-sectional slice at $x = 30$ mm for (a) $\Omega = 0$ and (b) $\Omega = 1$ at $N = 2$.

15475905, 1998, 6, Downloaded from https://aiche.onlinelibrary.wiley.com/doi/10.1002/aic.690440605 by Universitá© De Nantes, Wiley Online Library on [13/10/2026]. See the Terms and Conditions (https://onlinelibrary.wiley.com/terms-and-conditions) on Wiley Online Library for rules of use; OA articles are governed by the applicable Creative Commons License

striations, which persist until they become indistinguishable. Such patterns are found in the experimental structures of 60-μm particles mentioned earlier. The figure parts also indicate that although the drum has returned to the horizontal position, the material does not level out, as evidenced by the different depths of the cross-sectional slices. This observation mimics experimental results.

Conclusions

Particle dynamic simulations were applied to a 3-D drum to characterize flow and mixing in a rotating and rocking cylinder partially filled with inelastic, frictional, spherical particles. Solid rotating boundaries at both ends of the cylinder were used to facilitate comparisons with experiments. Velocity profiles generated in the simulation matched those found by MRI and video imaging. Similar to experimental results, axial composition profiles showed that addition of rocking motion to a rotating drum improved axial mixing compared to purely rotating motion. Linear density profiles also matched expected results. Particle dynamic simulations show promise for gaining insight into flows in more complicated geometries, such as V-blenders and 3-D funnel discharge. As computational capabilities are increased in the future, these more complicated velocity fields could be generated by DEM, and then placed into faster simulating techniques to understand increasingly complex powder-mixing processes.

Notation

F = force from applied loads
g = acceleration of gravity
K_2 = normal force unloading stiffness
M = number of particles in a zone
N_p = number of particles
r = position
v = velocity

Literature Cited

Allen, M. P., and D. J. Tildesley, *Computer Simulation of Liquids*, Oxford Univ. Press, New York (1987).

Bak, P., C. Tang, and K. Wiesenfeld, "Self-Organized Criticality," *Phys. Rev. A*, **38**(1), 364 (1988).

Barker, G. C., "Computer Simulations of Granular Materials," *Granular Matter: An Interdisciplinary Approach*, A. Mehta, eds., Springer-Verlag, New York, p. 35 (1994).

Baumann, G., I. M. Jánosi, and D. E. Wolf, "Surface Properties and Flow of Granular Material in a Two-Dimensional Rotating-Drum Model," *Phys. Rev. E*, **51**(3), 1879 (1995).

Baxter, G. W., R. P. Behringer, T. Fagert, and A. Johnson, "Pattern Formation in Flowing Sand," *Phys. Rev. Lett.*, **62**(24), 2825 (1989).

Baxter, G. W., R. Leone, and R. P. Behringer, "Experimental Test of Time Scales in Flowing Sand," *Europhys. Lett.*, **21**(5), 569 (1993).

Brone, D., C. Wightman, K. Connor, A. Alexander, F. J. Muzzio, and P. Robinson, "Using Flow Perturbations to Enhance Mixing of Dry Powders in V-Blenders," *Powder Technol.*, **91**, 165 (1997).

Buchholtz, V., T. Poschel, and H. Tillemans, "Simulation of Rotating Drum Experiments using Non-Circular Particles," *Physica A*, **216**, 199 (1995).

Chen, K., and P. Bak, "Self-Organized Criticality," *Sci. Amer.*, **264**, 46 (1991).

Cundall, P. A., and O. D. L. Stack, "A Discrete Numerical Model for Granular Assemblies," *Geotechnique*, **29**(1), 47 (1979).

Edwards, S. F., and C. C. Mounfield, "A Theoretical Model for the Stress Distribution in Granular Matter. I. Basic Equations," *Physica A*, **226**, 1 (1996).

Ennis, B. J., J. Green, and R. Davis, "The Legacy of Neglect in the US," *Chem. Eng. Prog.*, **90**, 32 (1994).

Evesque, P., and C. Stefani, "Relationship Between Dilatancy, Stresses and Plastic Dissipation in a Granular Material with Rigid Grains," *J. Phys. II France*, **1**, 1337 (1991).

Evesque, P., D. Fargeiz, P. Habib, M. P. Luong, and P. Porion, "Gravity and Density Dependences of Sand Avalanches," *J. Phys. I France*, **2**, 1271 (1992).

Ghaboussi, J., and R. Barbosa, "Three-Dimensional Discrete Element Method for Granular Materials," *Int. J. Num. Anal. Methods Geomech.*, **14**, 451 (1990).

Glanz, J., "Grown-up Physicists Play Serious Games in the Sandbox," *Science*, **268**, 1277 (1995).

Hill, K. M., and J. Kakalios, "Reversible Axial Segregation of Rotating Granular Media," *Phys. Rev. E*, **52**(4), 4393 (1995).

Hogg, R., and D. W. Fuerstenau, "Transverse Mixing in Rotary Cylinders," *Powder Technol.*, **6**, 139 (1972).

Hogg, R., D. S. Cahn, T. W. Healy, and D. W. Fuerstenau, "Diffusional Mixing in an Ideal System," *Chem. Eng. Sci.*, **21**, 1025 (1966).

Hogue, C., and D. Newland, "Efficient Computer Simulation of Moving Granular Particles," *Powder Technol.*, **78**, 51 (1994).

Jaeger, H. M., and S. R. Nagel, "Physics of the Granular State," *Science*, **255**, 1523 (1992).

Jaeger, H. M., S. R. Nagel, and R. P. Behringer, "The Physics of Granular Materials," *Phys. Today*, **49**(6), 32 (1996).

Johnson, P. C., P. Nott, and R. Jackson, "Frictional-Collisional Equations of Motion for Particulate Flows and Their Application to Chutes," *J. Fluid Mech.* **210**, 501 (1990).

Lacey, P. M., "The Mixing of Particles—The Application of Theory to Practice," *Chem. Age*, **53**, 119 (1945).

McCarthy, J. J., J. E. Wolf, T. Shinbrot, G. Metcalfe, and J. M. Ottino, "Mixing of Granular Material in Slowly Rotated Containers," *AIChE J.*, **42**, 3351 (1996).

Mehta, A., "Relaxation Dynamics, Avalanches, and Disorder in Real Sandpiles," *Granular Matter: An Interdisciplinary Approach*, A. Mehta, eds., Springer-Verlag, New York, p. 1 (1994).

Mishra, B. K., and R. K. Rajamani, "Motion Analysis in Tumbling Mills by the Discrete Element Method," *Powder Part.*, **8**, 92 (1990).

Nakagawa, M., S. A. Altobelli, A. Caprihan, E. Fukushima, and E.-K. Jeong, "Non-Invasive Measurements of Granular Flows by Magnetic Resonance Imaging," *Exp. Fluids*, **16**, 54 (1993).

Rajchenbach, J., E. Clement, and J. Duran, "Experimental Study of Bidimensional Models of Sand," *Int. J. Modern Phys. B*, 7(9 & 10), 1789 (1993).

Ristow, G. H., "Particle Mass Segregation in a Two-Dimensional Rotating Drum," *Europhys. Lett.*, **28**(2), 97 (1994).

Rose, H. E., and R. M. E. Sullivan, *A Treatise on the Internal Mechanics of Ball, Tube and Rod Mills*, Chem. Pub. Co., New York (1958).

Walton, O. R., and R. L. Braun, "Simulation of Rotary-Drum and Repose Tests for Frictional Spheres and Rigid Sphere Clusters," Joint DOE/NSF Workshop on the Flow of Particulates and Fluids, Ithaca, NY (1993).

Walton, O. R., and R. L. Braun, "Viscosity, Granular-Temperature, and Stress Calculations for Shearing Assemblies of Inelastic, Frictional Disks," *J. Rheol.*, **50**(5), 949 (1986).

Walton, O. R., "Numerical Simulation of Inclined Chute Flow of Monodisperse, Inelastic, Frictional Spheres," *Mech. Mater.*, **16**, 239 (1993a).

Walton, O. R., "Numerical Simulation of Inelastic, Frictional Particle-Particle Interactions," *Particulate Two-Phase Flow*, M. C. Roco, ed., Butterworth-Heinemann, Boston, p. 884 (1993b).

Wightman, C., and F. J. Muzzio, "Mixing of Granular Material in a Drum Mixer Undergoing Rotational and Rocking Motions: I. Uniform Particles," *Powder Technol.*, in press (1998).

Wightman, C., P. R. Mort, F. J. Muzzio, R. E. Riman, and E. K. Gleason, "The Structure of Mixtures of Particles Generated by Time-Dependent Flows," *Powder Technol.*, **84**, 231 (1995).

Wightman, C., F. J. Muzzio, and J. Wilder, "A Quantitative Image Analysis Method for Characterizing Mixtures of Granular Materials," *Powder Technol.*, **89**, 165 (1996).

Manuscript received Aug. 18, 1997, and revision received Dec. 1, 1997.

15475905, 1998, 6, Downloaded from https://aiche.onlinelibrary.wiley.com/doi/10.1002/aic.690440605 by Universitá© De Nantes, Wiley Online Library on [13/10/2026]. See the Terms and Conditions (https://onlinelibrary.wiley.com/terms-and-conditions) on Wiley Online Library for rules of use; OA articles are governed by the applicable Creative Commons License